Chinese Chemical Letters 36 (2025) 110139

Contents lists available at ScienceDirect

Chinese Chemical Letters

journal homepage: www.elsevier.com/locate/cclet

Al-O bridged $NiFeO_x/BiVO_4$ photoanode for exceptional photoelectrochemical water splitting

Lina Wang[a,d], Hairu Wang[a], Qian Bu[a], Qiong Mei[a], Junbo Zhong[c], Bo Bai[a], Qizhao Wang[a,b,*]

[a] School of Water and Environment, Key Laboratory of Subsurface Hydrology and Ecological Effects in Arid Region of Ministry of Education, Key Laboratory of Subsurface Hydrology and Ecological Effect in Arid Region of the Ministry of Education, Chang'an University, Xi'an 710054, China
[b] College of Chemistry and Chemical Engineering, Northwest Normal University, Lanzhou 730070, China
[c] Key Laboratories of Fine Chemicals and Surfactants in Sichuan Provincial Universities, Sichuan University of Science & Engineering, Zigong 643000, China
[d] School of Engineering and Management, Shanxi Vocational University of Engineering Science and Technology, Jinzhong 030619, China

ARTICLE INFO

Article history:
Received 14 February 2024
Revised 19 May 2024
Accepted 17 June 2024
Available online 18 June 2024

Keywords:
PEC
Photoanode
Bridge
OECs
Water splitting

ABSTRACT

Developing $BiVO_4$ photoanode with efficient carrier transfer and fast water oxidation kinetics is the permanent pursuit to achieve the state-of-art solar-driven photoelectrochemical (PEC) water splitting. The capacity to increase the PEC activity of $BiVO_4$ by loading oxygen evolution co-catalysts (OECs) has been proven, however it suffers from sluggish charge carriers dynamics brought on by the complicated interface between $BiVO_4$ and OECs as well as poor long-term durability. Herein, we connected OECs ($NiFeO_x$) and photoanode with a Al-O bridge for bettering the PEC performance of $BiVO_4$. The Al-O bridge served as a channel to extract hole from $BiVO_4$ to $NiFeO_x$, thus boosting charge carriers' separation and preventing $BiVO_4$ from photo-corrosion. The Al-O bridging photoanode ($NiFeO_x/Al_2O_3/BiVO_4$) demonstrated a high photocurrent density of 5.87 mA/cm^2 at 1.23 V *vs.* RHE and long-term photostability in comparison to $NiFeO_x/BiVO_4$ photoanode. This study proposes a unique technique to boost charge carriers' separation between $BiVO_4$ and OECs for high-efficiency solar-driven PEC water splitting.

Photoelectrochemical (PEC) water splitting has the potential to convert solar energy into sustainable hydrogen energy using semiconductor photocatalysts, thus realizing an efficient, green and carbon-free pathway for green hydrogen production [1,2]. Narrow-band-gap metal oxides such as WO_3 (~2.7 eV) [3-5], α-Fe_2O_3 (~2.2 eV) [5,6] and $BiVO_4$ (2.4 eV) [7,8] are frequently utilized as photoanodes due to their inexpensiveness, superior photoactivity and great photostability. In particular, monoclinic phase $BiVO_4$ is regarded as an excellent photoanode due to its non-toxicity, abundance, suitable band gap and valence band potential [9,10]. Unfortunately, the low photogenerated electron-hole separation efficiency and slow surface water splitting rate on $BiVO_4$ photoanode surface constrain the further improvement of solar-to-hydrogen (STH) efficiency [1,11]. Introducing oxygen evolution co-catalysts (OECs), especially binary or multi transition metal-based cocatalysts (such as $NiFe_2O_4/BiVO_4$, $CoFe_2O_4/BiVO_4$ [12] and $ZnCo_2O_4/BiVO_4$ [13]), helps to encourage the transfer and separation of charges, thereby enhancing charge injection efficiency and overall photocurrent density. However, the interface of OECs/$BiVO_4$ heterojunction usually acts as a charge recombination center, resulting in lower charge transfer efficiency and terrible long-term durability. Therefore, it is of particular interest to modify the interface between OECs and $BiVO_4$ photoanode that inhibits electron/hole pairs' recombination and accelerating water oxidation.

Introducing carrier shuttle bridge between OECs and $BiVO_4$ photoanode has shown to be a workable solution to eliminate the inherent charge transfer barriers [14-16]. For example, bridging the coordination of metal hydroxides and $BiVO_4$ photoanode with urea can achieve stable and efficient solar-driven PEC water splitting with a photocurrent density of 4.8 mA/cm^2 at 1.23 V *vs.* RHE [17]. This is due to the fact that metal ion and urea's strong coordination connection may prevent electron-hole pairs from recombining at the OECs/$BiVO_4$ heterojunction, increasing the transmission of charge to the water oxidation reactive sites. However, the reported PEC water splitting performance of $BiVO_4$-based photoanodes with the built charge shuttle bridge is far from satisfactory when compared with the theoretical photocurrent density of $BiVO_4$ photoanode (7.5 mA/cm^2) [18,19]. Searching a more efficeint charge shuttle

* Corresponding author.
E-mail addresses: qzwang@chd.edu.cn, wangqizhao@163.com (Q. Wang).

https://doi.org/10.1016/j.cclet.2024.110139
1001-8417/

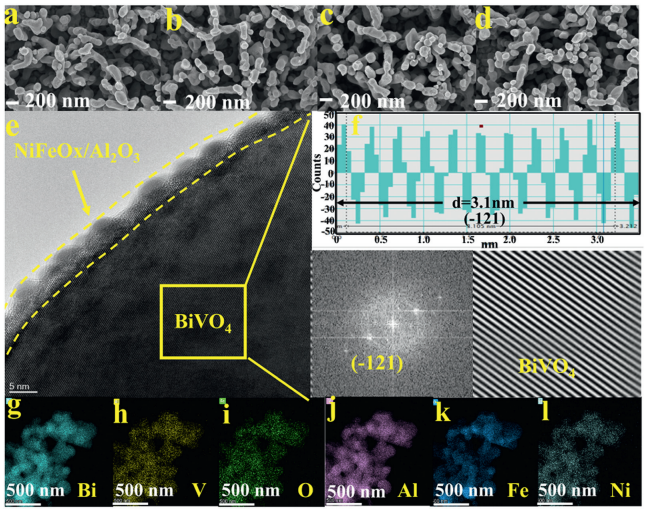

Fig. 1. Top-view SEM images of (a) $BiVO_4$, (b) $Al_2O_3/BiVO_4$, (c) $NiFeO_x/BiVO_4$ and (d) $NiFeO_x/Al_2O_3/BiVO_4$ photoanodes. HRTEM images (e, f) and TEM-EDS mapping images of $NiFeO_x/Al_2O_3/BiVO_4$ film (g-l).

bridge is thus of significance and urgency. Aluminum oxide (Al_2O_3) is a polycrystalline structure which is composed by oxygen and aluminum atoms through ionic and covalent bonds [20-22]. Consequently, the $NiFeO_x/BiVO_4$ photoanode modified with Al-O bridge is expected to achiesubstantially improved PEC water splitting performance by virtue of the good light transmission and extremely high chemical stability [23,24].

Herein, we successfully bridged $NiFeO_x$ and $BiVO_4$ with the Al-O unit through a facile impregnation method. Benefiting from the dual improved carrier charge transport by the co-loaded $NiFeO_x$ and Al_2O_3, this novel Al-O bridged $NiFeO_x/BiVO_4$ photoanode achieved an impressive photocurrent density of 5.87 mA/cm^2 at 1.23 V *vs.* RHE. A stoichiometric hydrogen and oxygen evolution of 222.64 μmol/cm^2 and 110.31 μmol/cm^2 achieved over Al-O bridged $NiFeO_x/BiVO_4$ photoanode, which is 2.26 and 18.06 times more than $NiFeO_x/BiVO_4$ and pristine $BiVO_4$ photoanode, respectively. This effort delivers a novel perspective to manipulate the interface of OECs/$BiVO_4$ photoanode for highly efficient solar-driven PEC water splitting.

The surface morphology and microstructure of the prepared films were investigated by scanning electron microscopy (SEM). From the top view (Fig. 1a and Fig. S1 in Supporting information) and the corresponding side view (Fig. S2a in Supporting information), a uniform layer of $BiVO_4$ with irregular particles between 200 nm and 500 nm has been successfully grown uniformly on the FTO and in close contact with it. The surface and side SEM images of $Al_2O_3/BiVO_4$, $NiFeO_x/BiVO_4$, $NiFeO_x/Al_2O_3/BiVO_4$ photoanodes are shown in Figs. 1b-d and Figs. S2b-d (Supporting information), respectively, which show that they are highly similar to the morphology of $BiVO_4$ nanoparticles with or without the introduction of Al_2O_3 and $NiFeO_x$, indicating that the morphology of the original $BiVO_4$ nanoparticles is not changed by the simple preparation process. In order to further understand the microstructure of $NiFeOx/Al_2O_3/BiVO_4$ photoanodes, a detailed study was carried out using transmission electron microscopy (TEM) and high resolution transmission electron microscope (HRTEM). The $BiVO_4$ has a granular morphology in Fig. 1e and Fig. S3 (Supporting information) and an amorphous/disordered layer appears at the edge of $BiVO_4$, indicating that $NiFeO_x$ and Al_2O_3 are coated on the surface of $BiVO_4$ particles. Further, a clearer HRTEM image of the $NiFeOx/Al_2O_3/BiVO_4$ photoanodes and the corresponding crystal plane spacing measurements were obtained in Fig. 1f by inverse Fourier transform, the spacing of the 10 ordered photoanodes was measured to be 3.1 nm, which represents the lattice stripe $d = 0.31$ nm matching the $(\bar{1}21)$ crystal plane of $BiVO_4$. The component mapping and energy dispersive X-Ray spectroscopy (EDX) distribution of $NiFeO_x/Al_2O_3/BiVO_4$ shows that Ni, Fe, Al, Bi, V and O components are evenly scattered in the nanomorphology of the sample (Figs. 1g-l and Fig. S4 in Supporting information), which further confirms that we have successfully combined $NiFeO_x/Al_2O_3/BiVO_4$ photoanodes by a simple process.

To further investigate the structures of $BiVO_4$, $Al_2O_3/BiVO_4$, $NiFeO_x/BiVO_4$, $NiFeO_x/Al_2O_3/BiVO_4$ samples, X-ray diffraction (XRD) analysis was performed in Fig. S5 (Supporting information). All samples give similar diffraction peaks as monoclinic phase scheelite $BiVO_4$ (JCPDS No. 14–0688), appearing at 2θ of 18.6°, 18.9°, 28.9°, 30.5°, 35.2°, 47.2° and 53.1°, corresponding to (110), (011), (121), (040), (002), (042), (222) crystallographic planes of $BiVO_4$, respectively [25]. No characteristic peaks of Al_2O_3 and $NiFeO_x$ were observed, probably due to the thinness of the loaded Al_2O_3 and $NiFeO_x$ layers or amorphous state, which is consistent with the TEM test results.

To further reveal the surface chemistry and bonding state of the elements, X-ray photoelectron spectroscopy (XPS) analysis was performed on $NiFeO_x/Al_2O_3/BiVO_4$ and $NiFeO_x/BiVO_4$ photoanodes. According to Fig. S6 (Supporting information), the XPS spectrum reveals the following elements in the sample: Bi, V, O, Al, Ni and Fe. As far as XPS spectra are concerned, there are no noticeable change in position or intensity of Bi and V elements before and after the introduction of the Al_2O_3 interlayer in Figs. 2a and b. There are two peaks at 529.7 eV and 531.7 eV in the O 1s XPS spectra in Fig. 2c, corresponding to the binding energy of lattice oxygen and hydroxyl adsorbed oxygen [26,27], respectively. The intensity of the lattice oxygen peak is significantly higher in $NiFeO_x/Al_2O_3/BiVO_4$ than in $NiFeO_x/BiVO_4$ sample, which is associated with Al_2O_3. Significantly, Al 2p signals were detected at 74.5 eV and 69.7 eV in Fig. 2d, which correspond to Al^{3+} in Al_2O_3 and Al^{3+} in tetrahedral positions [28,29], respectively. The presence of $NiFeO_x$ is further confirmed by the observation of faint Fe and Ni signals in Figs. 2e and f. Compared with the $NiFeO_x/BiVO_4$ sample, a shift of Fe and Ni binding energy to lower binding energy was observed in the $NiFeO_x/Al_2O_3/BiVO_4$ photoanode, revealing an off-domain effect due to the electron shuttle bridge Al_2O_3 to adjust the $NiFeO_x/Al_2O_3/BiVO_4$ to the lowest energy [24,29,30]. The XPS results suggest that Al_2O_3 was successfully integrated into the $NiFeO_x/BiVO_4$ anode as an efficient bridge for charge transfer and further validate the successful synthesis of $NiFeO_x/Al_2O_3/BiVO_4$ photoanode.

By using 1 mol/L potassium borate buffer (KPi, pH 9.5) and AM 1.5G (100 mW/cm^2), the PEC performance of the as-prepared $BiVO_4$ photoanodes was tested by linear scanning voltammetry (LSV). The photocurrent density of unmodified $BiVO_4$ was 1.65 mA/cm^2 at 1.23 V *vs.* RHE in Fig. 3a. Such low current density was ascribed by the severe charge recombination and low surface charge transport [25,31]. The photocurrent density rose to 3.26 mA/cm^2 when $BiVO_4$ was loaded by Al_2O_3 (Fig. S7 in Supporting information). The photocurrent densities of the prepared $NiFeO_x/BiVO_4$ and $NiFeO_x/Al_2O_3/BiVO_4$ photoanodes were significantly increased after the $NiFeO_x$ co-catalyst was loaded, which is backed up by the recent literature claim that $NiFeO_x$ co-catalyst can improve $BiVO_4$ photoanode PEC water oxidation activity [32,33]. Differently, the prepared $NiFeO_x/Al_2O_3/BiVO_4$ film exhibit a significant photocurrent density of 5.87 mA/cm^2 at 1.23 V *vs.* RHE, which is nearly 1.4 times greater than that of $NiFeO_x/BiVO_4$ (4.21 mA/cm^2) and 3.5 times higher than that of pure $BiVO_4$. The presence of the Al_2O_3 intermediate layer and the synergistic effect of the $NiFeO_x$ co-catalyst might be the cause of the higher photocurrent density in the $NiFeO_x/Al_2O_3/BiVO_4$ system. To further reveal the response

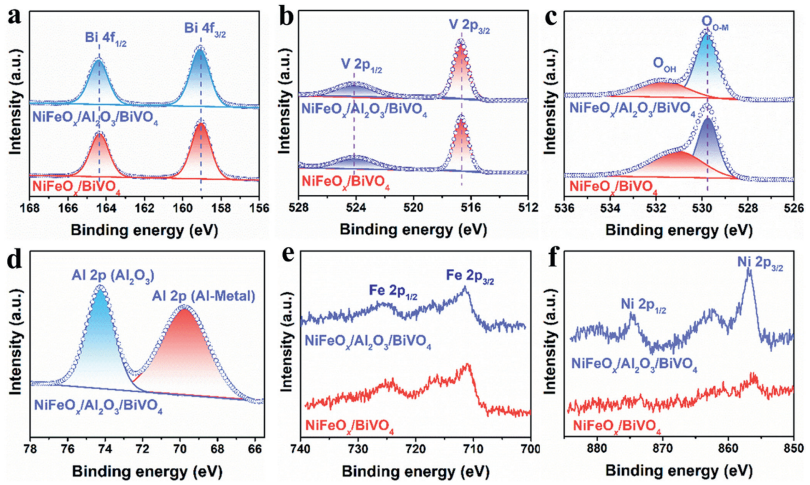

Fig. 2. (a) Bi 4f, (b) V 2p, (c) O 1s, (d) Al 2p, (e) Fe 2p and (f) Ni 2p XPS spectra of $NiFeO_x/BiVO_4$ and $NiFeO_x/Al_2O_3/BiVO_4$.

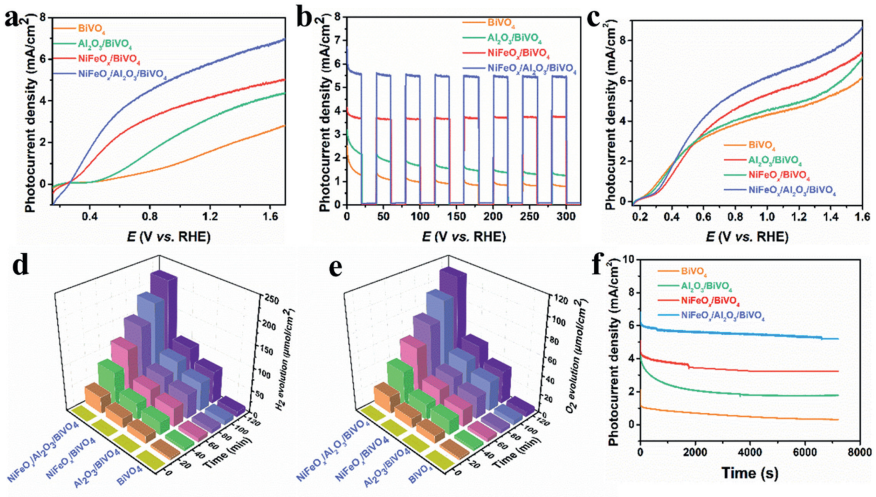

Fig. 3. PEC performance of $BiVO_4$, $Al_2O_3/BiVO_4$, $NiFeO_x/BiVO_4$ and $NiFeO_x/Al_2O_3/BiVO_4$ photoanodes: (a) Linear-sweep voltammogram curves at scan rate of 50 mV/s. (b) Transient photocurrent (*i-t*) spectra at 1.23 V *vs.* RHE, (c) LSV curves in the presence of 1 mol/L Na_2SO_3 with a scan rate of 50 mV/s. H_2 (d) and O_2 (e) gas evolution from PEC water splitting in a 1.0 mol/L potassium borate buffer solution electrolyte. (f) Long-time *i-t* spectra of H_2 and O_2 production of $NiFeO_x/Al_2O_3/BiVO_4$ photoanode.

of the photoanode to light under illumination with the transfer and separation of carriers, we performed transient photocurrent tests. The rapid change of photocurrent density implies a very fast charge transfer in the photoanode. It is clearly observed that the current density of $NiFeO_x/Al_2O_3/BiVO_4$ photoanode is the strongest and more stable after compounding $NiFeO_x$ and Al_2O_3 in Fig. 3b, which is the same as the previous experimental results of LSV. Assumedly, photogenerated holes on the electrode surface can be 100% injected into the electrolyte because Na_2SO_3 is oxidized by holes so quickly [34]. The LSV curves of the prepared $BiVO_4$ photoanodes were tested under the conditions of 1 mol/L phosphate buffer (KPi, pH 9.5) electrolyte with the addition of Na_2SO_3 in Fig. 3c. The trends of the photocurrent densities were the same and increased for all photoanodes, indicating that the photoanode suffered from a severe recombination of electrons and holes for PEC water splitting performance.

To further demonstrate that the measured photogenerated currents were used for the PEC water splitting of hydrogen and oxygen production, the hydrogen and oxygen produced by $BiVO_4$, $Al_2O_3/BiVO_4$, $NiFeO_x/BiVO_4$ and $NiFeO_x/Al_2O_3/BiVO_4$ photoanodes were quantified using gas chromatography. The Figs. 3d and e demonstrate that the gas precipitation from all photoanodes showed an increasing trend with time. After 120 min of continuous light exposure to the PEC decomposition water reaction, the yields of H_2 and O_2 from $BiVO_4$, $Al_2O_3/BiVO_4$, $NiFeO_x/BiVO_4$ and $NiFeO_x/Al_2O_3/BiVO_4$ photoanodes were 12.33 and 5.66 μmol/cm^2, 72.14 and 35.06 μmol/cm^2, 98.42 and 49.07 μmol/cm^2 and 222.64 and 110.31 μmol/cm^2, respectively (Fig. S9 in Supporting information). The $NiFeO_x/Al_2O_3/BiVO_4$ photoanode for PEC decomposition of water performance was nearly 18 times that of the blank $BiVO_4$, which verified the feasibility of our design using Al_2O_3 as an electron shuttle bridge and the introduction of $NiFeO_x$ co-catalyst for improving $BiVO_4$'s PEC performance. In the meanwhile, the photoelectrodes' stability test revealed that after 120 min of exposure to light at 1.23 V *vs.* RHE, the photocurrent density of the $NiFeO_x/Al_2O_3/BiVO_4$ electrode was greater than that of $BiVO_4$, indicating a significant enhancement of the photostability of $NiFeO_x/Al_2O_3/BiVO_4$ (Fig. 3f). Meanwhile, the XRD pattern and SEM in Fig. S10 (Supporting information) showed little change in the $NiFeO_x/Al_2O_3/BiVO_4$ photoanode morphology before and after the test, further confirming the enhanced stability of the $BiVO_4$ photoanode after deposition of $NiFeO_x$ and Al_2O_3. Therefore, the $NiFeO_x/Al_2O_3/BiVO_4$ thin film not only can avoid the oxidation of $BiVO_4$, but also can promote the transfer of carriers to the electrolyte solution, thus promoting the release of hydrogen and oxygen.

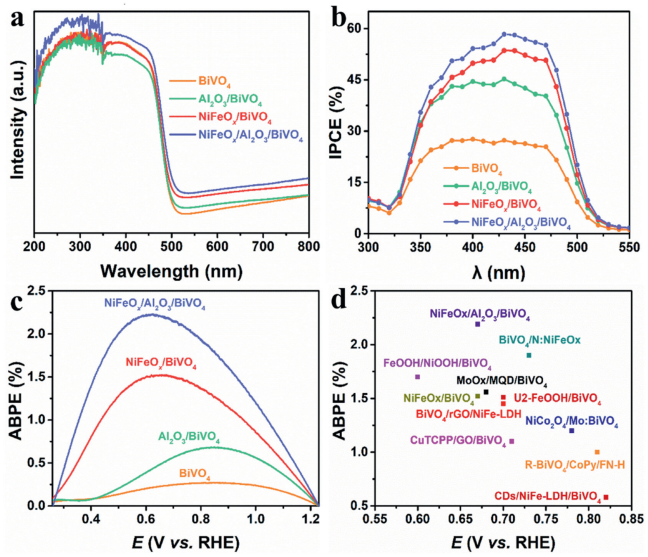

Fig. 4. The Optical properties and PEC properties of $BiVO_4$, $Al_2O_3/BiVO_4$, $NiFeOx/BiVO_4$ and $NiFeOx/Al_2O_3/BiVO_4$ photoanodes: (a) the UV–vis absorption spectra; (b) IPCE curves at 1.23 V *vs.* RHE; (c) ABPE curves and (d) the ABPE of different photoelectrodes under AM1.5G illumination.

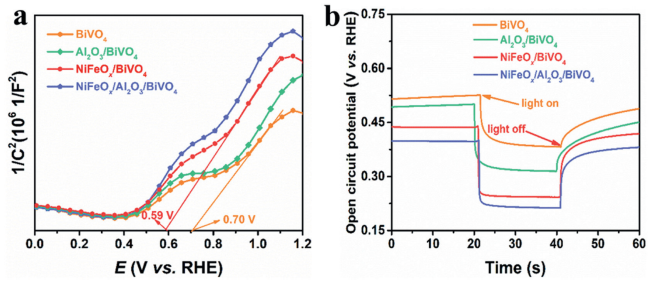

Fig. 5. Carrier transport performance of $BiVO_4$, $Al_2O_3/BiVO_4$, $NiFeO_x/BiVO_4$ and $NiFeO_x/Al_2O_3/BiVO_4$ photoanodes: (a) Mott-Schottky curves under dark; (b) Open circuit potential measurements.

UV–vis absorption spectra were used to check the synthetic photoanodes' capacity to absorb light. In accordance with other results [18,31], Fig. 4a demonstrates that $BiVO_4$ exhibits a considerable light absorption at a wavelength of around 500 nm. The light absorption of $BiVO_4$ photoanode has been slightly broadened after the introduction of Al_2O_3 and $NiFeO_x$. Correspondingly, the optical bandgaps of $BiVO_4$, $Al_2O_3/BiVO_4$, $NiFeO_x/BiVO_4$ and $NiFeO_x/Al_2O_3/BiVO_4$ calculated by Tauc method are 2.47 eV, 2.46 eV, 2.46 eV and 2.43 eV, respectively (Fig. S11 in Supporting information). As a result, the $NiFeO_x/Al_2O_3/BiVO_4$ photoanode's improvements in PEC water splitting activity are not primarily influenced by the energy band structure of the photoanodes. PEC activity and incident light wavelength can be related to one other using observations of incident photon to current conversion efficiency (IPCE) in Fig. 4b. Pure $BiVO_4$ shows the lowest IPCE value in the 300–550 nm. However, the IPCE value increased and reached 45% at 430 nm for $Al_2O_3/BiVO_4$. Similarly, the IPCE values of $NiFeO_x/BiVO_4$ and $NiFeO_x/Al_2O_3/BiVO_4$ show a further increase. In particular, the $NiFeO_x/Al_2O_3/BiVO_4$ shows the largest IPCE value of 58% at 430 nm, demonstrating that $NiFeO_x$ and Al_2O_3 do not expand the light absorption, but can significantly increase the efficiency of solar energy conversion and the interfacial separation of photogenerated carriers. The applied bias photon-to-current efficiency (ABPE) was computed from the LSV curve to describe the solar water splitting half-reaction hydrogen precipitation efficiency. Accordingly, the $NiFeO_x/Al_2O_3/BiVO_4$ photoanode has a higher photoelectric conversion efficiency in the whole applied bias range and attains an ABPE of 2.19% at 0.67 V *vs.* RHE in Fig. 4c, further supporting the claim that combining $NiFeO_x$ and Al_2O_3 is a successful method for enhancing $BiVO_4$'s PEC performance with higher photoelectric conversion efficiency at lower potentials. In comparison, this was found to be an extremely high level among the many photoanodes reported so far (Fig. 4d) [35-38].

Based on the aforementioned experimental results, the values of surface charge injection efficiency (η_{inj}) and bulk phase charge separation efficiency (η_{sep}) of the samples were determined. Compared with the pure $BiVO_4$ photoanode, the η_{inj} of $Al_2O_3/BiVO_4$, $NiFeO_x/BiVO_4$ and $NiFeO_x/Al_2O_3/BiVO_4$ have significantly improved in the overall bias voltage range in Fig. S12a (Supporting information), especially for the $NiFeO_x/BiVO_4$ electrode. The η_{inj} of $NiFeO_x/BiVO_4$ shows a decreasing trend when the bias voltage is >1.3 V *vs.* RHE, indicating that the water oxidation reaction at the interface has almost reached saturation at this time [39], further demonstrating the effectiveness of $NiFeO_x$ in accelerating the water oxidation reaction kinetics. The η_{sep} follows a similar pattern with η_{sep} reaching 74.4% for $NiFeO_x/BiVO_4$ and 62.4% for $Al_2O_3/BiVO_4$ at 1.23 V *vs.* RHE in Fig. S12b (Supporting information), both of which are much greater than $BiVO_4$ (59.3%). After introducing Al_2O_3 between $NiFeO_x/BiVO_4$, the η_{sep} of $NiFeO_x/Al_2O_3/BiVO_4$ is increased to 85.2% at 1.23 V *vs.* RHE, indicating that Al_2O_3 forms a fast transport channel for photogenerated electrons, reducing their chance of recombination in the bulk phase. Electrochemical impedance spectroscopy (EIS) measurements were carried out in Fig. S12c (Supporting information) under visible light irradiation to acquire a better understanding of the electron transfer kinetics. From the impedance diagrams of Fig. S12c and simulated impedance values of Table S1 (Supporting information), the impedances of $Al_2O_3/BiVO_4$, $NiFeO_x/BiVO_4$ and $NiFeO_x/Al_2O_3/BiVO_4$ photoanodes are all reduced compared to the original $BiVO_4$ photoanode, suggesting that the addition of both Al_2O_3 and $NiFeO_x$ helps to improve the electrical conductivity of the $BiVO_4$ photoanode while the addition of Al_2O_3 optimizes the contact between NiFeOx and $BiVO_4$ substrate, which may be one of the reasons for its high photocurrent density. To demonstrate the charge transport mechanism of $BiVO_4$, $Al_2O_3/BiVO_4$, $NiFeO_x/BiVO_4$ and $NiFeO_x/Al_2O_3/BiVO_4$ photoanodes, the room temperature steady-state PL were characterized in Fig. S12d (Supporting information). As a consequence, $BiVO_4$ showed a signal peak in the wavelength range around 500 nm, which may be due to the emission of the $BiVO_4$ band gap jump. Likewise, the signal peaks of $Al_2O_3/BiVO_4$, $NiFeO_x/BiVO_4$ and $NiFeO_x/Al_2O_3/BiVO_4$ showed no change in position but the intensity of the emission peak was significantly reduced, indicating that the $NiFeO_x/Al_2O_3/BiVO_4$ photoanode could prevent the photogenerated electron-hole pair recombination.

Mott-Schottky (M-S) experiments were performed in Fig. 5a to further study the intrinsic electronic structure of the photoanodes. The positive slopes of the M-S curves show that these photoanodes are n-type semiconductors with a high proportion of migrating electrons. The carrier concentrations of $BiVO_4$, $Al_2O_3/BiVO_4$, $NiFeO_x/BiVO_4$ and $NiFeO_x/Al_2O_3/BiVO_4$ photoanodes were calculated to be 2.91×10^{21}, 3.12×10^{21}, 3.21×10^{21} and 3.97×10^{21} cm^{-3} in Table S2 (Supporting information), respectively. The carrier concentration did not change significantly and also verified that the Al, Ni and Fe ions were not doped into the $BiVO_4$ photoanode during the loading of Al_2O_3 and $NiFeO_x$. The OCP curves were obtained by rapidly switching off the light source after reaching steady state at the open circuit voltage to analyze the mechanism of charge separation. In Fig. 5b, two decay process are observed after switching off the light. The instantaneous rise in voltage indicates that part of the electrons has returned to the semiconductor's valence band (VB), while the other part is captured

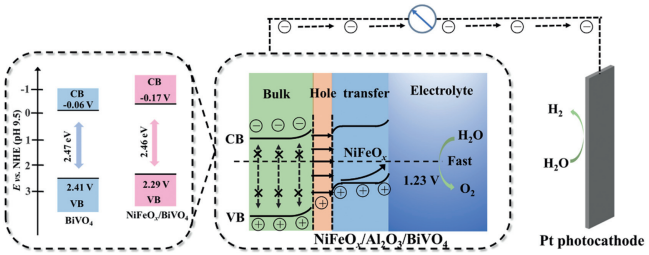

Fig. 6. The mechanism of $NiFeO_x/Al_2O_3/BiVO_4$ photoanode for PEC water splitting.

and recombinated with holes. The later, slowly decaying process represents the injection of charge into the electrolyte. Compared to the other samples, the $NiFeO_x/Al_2O_3/BiVO_4$ photoanode has a more positive potential value of 0.21 V *vs.* RHE, while the $BiVO_4$ film has a potential value of 0.38 V *vs.* RHE, further demonstrating that the co-addition of $NiFeO_x$ and Al_2O_3 can accelerate the aggregation of photogenerated electrons at the conduction band (CB) of $BiVO_4$, which in turn induces the $NiFeO_x/Al_2O_3/BiVO_4$ surface electron-hole pair separation.

The energy band structure of the $BiVO_4$ and $NiFeO_x/BiVO_4$ samples was investigated to study and clarify the reaction mechanism for PEC water splitting. In the M-S curve, the intersection of the tangent line with the *x*-axis ($y = 0$) is the flat-band potential. The flat-band potential is 0.2 V higher than the CB potential for n-type semiconductors, so the CBs of $BiVO_4$ and $NiFeO_x/BiVO_4$ photoanodes are −0.06 V *vs.* NHE and −0.17 V *vs.* NHE ($E_{RHE} = E_{NHE} + pH \times 0.059$). After combining with the previously obtained data on the forbidden band width of the films, a schematic energy band structure of the as-prepared films is obtained. From the Fig. 6, it can be found that the CB and VB of $BiVO_4$ films are gradually shifted to lower energy levels with the addition of $NiFeO_x$. Such a structure not only allows the excited holes of VB of $BiVO_4$ to be transferred to the aqueous solution, but also keeps the photogenerated electrons in $BiVO_4$'s CB.

Based on the above experimental results, we propose the mechanism of charge separation and transfer at $NiFeO_x/Al_2O_3/BiVO_4$ electrodes in the PEC water splitting process (Fig. 6). The energy band structure of $NiFeO_x$ was adopted from previous reports [40,41]. The electrons stored in the $BiVO_4$ photoanode are also rapidly released and transmitted to the Pt photocathode, where they reduce water to produce H_2. The holes remaining in the VB of the $BiVO_4$ photoanode will be rapidly transferred to the $NiFeO_x$ surface *via* the Al-O bridge, then transferred to the electrolyte solution for the oxidation reaction. At the same time, the Al-O bridge acts as a channel to speed up the transmission of holes from the $BiVO_4$ photoanode to the $NiFeO_x/Al_2O_3/BiVO_4$ photoanode surface. Therefore, the excellent PEC water splitting performance of $NiFeO_x/Al_2O_3/BiVO_4$ photoanode depends on the dual improvement of carrier transfer both within the photoanode and between the photoanode and electrolyte when $NiFeO_x$ and Al_2O_3 are co-loaded.

To address the shortcomings of $BiVO_4$ photoanode that electrons and holes are easily compounded, $NiFeO_x/Al_2O_3/BiVO_4$ photoanode was successfully designed and prepared by compounding the interlayer Al_2O_3, which significantly improved the PEC performance of $BiVO_4$. The $NiFeO_x/Al_2O_3/BiVO_4$ photoanode not only maintains high chemical stability, but also achieves a water oxidation photocurrent density of 5.87 mA/cm^2 (1.23 V *vs.* RHE) and an ABPE value of 2.19% (0.67 V *vs.* RHE), respectively, a 3.5-fold improvement over $BiVO_4$ (1.65 mA/cm^2) and 8.1 times better than $BiVO_4$ (0.27%). By modifying the Al_2O_3 layer with a $NiFeO_x$ co-catalyst, the holes are rapidly transferred to the $NiFeO_x$ surface for the water oxidation reaction, which reduces the interfacial charge recombination, regulates carrier concentration, effectively promotes charge separation and improves the stability of PEC water splitting. This research offers fresh perspectives and takeaways for the practical use of solar-powered PEC water splitting systems.

Declaration of competing interest

All authors declared that they do not have any commercial or associative interest that represents a conflict of interest in connection with the work submitted.

CRediT authorship contribution statement

Lina Wang: Writing – original draft, Writing – review & editing. **Hairu Wang:** Data curation, Writing – review & editing. **Qian Bu:** Writing – review & editing. **Qiong Mei:** Data curation, Methodology, Writing – review & editing. **Junbo Zhong:** Supervision, Writing – review & editing. **Bo Bai:** Resources, Supervision. **Qizhao Wang:** Funding acquisition, Resources, Supervision, Writing – review & editing.

Acknowledgments

This work was financially supported by the National Natural Science Foundation of China (No. 52173277), the Fundamental Research Funds for the Central Universities of Chang'an University (No. 300102299304), the Innovative Research Team for Science and Technology of Shaanxi Province (No. 2022TD-04) and the open program of Key Laboratories of Fine Chemicals and Surfactants in Sichuan Provincial Universities (No. 2023JXZ03).

Supplementary materials

Supplementary material associated with this article can be found, in the online version, at doi:10.1016/j.cclet.2024.110139.

References

[1] X. Meng, C. Zhu, X. Wang, et al., Nat. Commun. 14 (2023) 2643.
[2] M. Liu, G. Zhang, X. Liang, et al., Angew. Chem. Int. Ed. 135 (2023) e202304694.
[3] W. Zhang, M. Tian, H. Jiao, et al., Chin. J. Catal. 43 (2022) 2321–2331.
[4] H. Sun, W. Hua, Y. Li, et al., ACS Sustain. Chem. Eng. 8 (2020) 12637–12645.
[5] F. Xiao, R. Guo, X. He, et al., Int. J. Hydrogen Energy 46 (2021) 7954–7963.
[6] N. Duc Quang, P. Cao Van, S. Majumder, et al., J. Colloid Interface Sci. 616 (2022) 749–758.
[7] V. Andrei, G.M. Ucoski, C. Pornrungroj, et al., Nature 608 (2022) 518–522.
[8] H. Bai, F. Wang, Z. You, et al., Colloids Surf. A 640 (2022) 128412.
[9] J. Zhang, X. Wei, J. Zhao, et al., Chem. Eng. J. 454 (2023) 140081.
[10] W. Zhou, T. Jiang, Y. Zhao, et al., J. Colloid Interface Sci. 549 (2019) 42–49.
[11] W. Bai, Y. Zhou, G. Peng, et al., Appl. Catal. B 315 (2022) 121606.
[12] Q. Wang, J. He, Y. Shi, et al., Appl. Catal. B 214 (2017) 158–167.
[13] J. Huang, Y. Wang, K. Chen, et al., Chin. Chem. Lett. 33 (2022) 2060–2064.
[14] Y. Dou, X. Yang, Q. Wang, et al., J. Colloid Interface Sci. 644 (2023) 256–263.
[15] X. Wang, H. Jiang, M. Zhu, et al., Chin. Chem. Lett. 34 (2023) 107683.
[16] X. Xu, H. Wang, K. Chen, et al., Chem. Eng. J. 485 (2024) 149922.
[17] M. Sun, C. Yuan, R.T. Gao, et al., Chem. Eng. J. 426 (2021) 131062.
[18] Y. Li, Q. Wang, X. Hu, et al., Chem. Eng. J. 433 (2022) 133592.
[19] Y. Long, H. Xu, J. He, et al., Surf. Interfaces 31 (2022) 102056.
[20] Z. Liu, G. Xu, L. Zeng, et al., Appl. Catal. B 324 (2023) 122259.
[21] Y. Zhang, M. Choi, Z. Wang, et al., Appl. Surf. Sci. 609 (2023) 155295.
[22] D.H.K. Jackson, T.F. Kuech, J. Power Sources 365 (2017) 61–67.
[23] R. Rajendiran, P.K. Seelam, A. Patchaiyappan, et al., Chem. Eng. J. 451 (2023) 138507.
[24] Y. Zhao, G. Liu, H. Wang, et al., J. Mater. Chem. A 9 (2021) 11285–11290.
[25] L. Wang, Z. Liu, J. Zhang, et al., Chin. Chem. Lett. 34 (2023) 108007.
[26] W. Chen, J. Du, H. Zhang, et al., Chin. Chem. Lett. 35 (2024) 109168.
[27] H. Ming, X. Bian, J. Cheng, et al., Appl. Catal. B 341 (2024) 123314.
[28] Z. Boukha, J.L. Ayastuy, A. Iglesias-González, et al., Appl. Catal. B 160-161 (2014) 629–640.

[29] Z. Zhou, S. Wu, L. Li, et al., ACS Appl. Mater. Interfaces 11 (2019) 5978–5988.
[30] J. Wang, C. Qin, H. Wang, et al., Appl. Catal. B 221 (2018) 459–466.
[31] K. Chen, R. Wang, Q. Mei, et al., Appl. Catal. B 344 (2024) 123670.
[32] L. Ling, C. Yuan, Q. Xu, et al., Surf. Interfaces 36 (2023) 102483.
[33] S. Wang, T. He, P. Chen, et al., Adv. Mater. 32 (2020) 2001385.
[34] L. Wang, H. Cheng, Z. Zhang, et al., Chem. Eng. J. 456 (2023) 140990.
[35] C. Feng, Q. Zhou, B. Zheng, et al., J. Mater. Chem. A 7 (2019) 22274–22278.
[36] X. Ning, B. Lu, Z. Zhang, et al., Angew. Chem. Int. Ed. 58 (2019) 16800–16805.
[37] H. Chen, S. Wang, J. Wu, et al., J. Mater. Chem. A 8 (2020) 13231–13240.
[38] S. Wang, P. Chen, Y. Bai, et al., Adv. Mater. 30 (2018) 1800486.
[39] Y. Wang, J. Huang, L. Wang, et al., Chin. J. Struct. Chem. 41 (2022) 2201054–2201068.
[40] S. Seenivasan, S. Adhikari, D.H. Kim, Chem. Eng. J. 422 (2021) 130137.
[41] F. Ning, M. Shao, S. Xu, et al., Energy Environ. Sci. 9 (2016) 2633–2643.